Journal of Engineering and Applied Sciences 15 (1): 319-326, 2020
ISSN: 1816-949X

A Study on the Limitations of GPR Exploration in Sand Layer Through Analysis of the Ground Subsidence Mechanism

Y. Han
Geotechnical Engineering Research Institute, Korean Geotechnical Society, Seoul, South Korea

Abstract: With the increased development of underground spaces in urban areas, ground subsidence has become an issue around the globe. In Korea, a law that specifies a systematic underground safety management procedure has been enacted with the goal of preventing ground subsidence accidents in urban areas. A number of methods can be used to find the fundamental cause of the occurrence of ground subsidence. Of these, a method based on GPR exploration has been actively studied in recent years. However, the GPR exploration method is significantly affected by the electromagnetic characteristics of the medium and the electromagnetic characteristics of various and complex elements of ground need to be analyzed through an accurate analysis of the ground subsidence mechanism. Therefore, in this study, GPR exploration simulation was conducted by analyzing the ground subsidence mechanism depending on the change in the groundwater level. In the sand layer, the boundary between the unsaturated and saturated ground showed a difference under high frequency, as electromagnetic waves were reflected due to the permittivity difference. Below the groundwater level, the attenuation of electromagnetic waves was large due to high electric conductivity. An underground cavity shape with a diameter of 0.5 m that is located 1.5 m below the ground showed a parabolic form. However, it was difficult to judge the presence of an underground cavity because a slight parabolic form was observed due to the overlapping of reflected signals when the vicinity of the underground cavity was relaxed depending on the change in the groundwater level.

Key words: Ground subsidence, GPR (Ground Penetrating Radar), electromagnetic characteristics, sand layer, underground cavity, management

INTRODUCTION

Ground subsidence refers to the sinking of the Earth's surface caused by the loss of the soil constituting ground due to a certain artificial stimulus in the ground. Ground subsidence is induced by artificial stimuli such as the leakage of water supply/sewage pipes and groundwater disturbance. Such artificial stimuli are different from a sinkhole where the sinking of the Earth's surface is induced by the cavity formed due to the melting of limestone in the ground with limestone bedrock (Han and Hwang, 2017).

In recent underground development in the urban areas of Korea, damages to surrounding buildings have frequently led to many complications with civil complaints and compensation issues. Moreover, the collapse of some buildings has resulted in the loss of both human lives and property. Accordingly, the central government has legislated the special act on underground safety management which took effect from January 1, 2018. This law specifies an underground safety management system for securing underground safety, under which underground safety impact assessment is performed for projects involving underground excavation work that exceeds a certain size. The law also calls for safety inspections to be regularly performed for underground facilities and the surrounding ground (Han, 2018).

Representative methods for exploring the Earth's subsurface include Ground Penetrating Radar (GPR) exploration, surface wave exploration and resistivity survey. Among them, the GPR exploration method is widely used for exploring shallow ground and structures using electromagnetic pulses. It also has outstanding applicability to environmental pollution zone surveys, ground surveys and nondestructive structure inspections (Reynolds, 2011). The factors affecting GPR signals include permittivity, electric conductivity and transmittance depending on the underground medium and the energy of electromagnetic waves can become relatively weak depending on the electrical characteristics. As mentioned above, GPR exploration is significantly affected by the electromagnetic characteristics of the underground medium. In the case of soil that is an underground medium, soil particles can be easily separated as they represent a discontinuum and interparticle displacement can easily occur when exposed to external force. In addition, the engineering property of

soil is characterized by heterogeneity and anisotropy. Thus, it includes diverse and complex elements depending on the depth of the ground.

In this study, the limitations of GPR exploration for underground safety inspection are analyzed based on a case analysis of ground subsidence mechanism induced by an artificial stimulus.

Analysis of the ground subsidence mechanism: Many researchers have made various attempts to investigate the ground subsidence mechanism through model experiments. Oh *et al*. (2016) performed an indoor model experiment for a scenario in which leakage occurred due to a sewage pipe defect. In the above experiment, the shape of the ground subsidence and the degree of sinking could be measured depending on the relative density of the ground and the location of the sewage pipe defect when continuous leakage occurred through a sewage pipe. The results showed that the defect at the lower part of the sewage pipe induced more damage to the ground than the defect at the upper part of the sewage pipe.

Kweon *et al*. (2016) observed the behavior of ground subsidence depending on various scenarios through a model experiment. In the above experiment, ground subsidence was observed by discharging water and earth/sand through a hole with a width of 5 mm at the center of the bottom of a soil box. The scenarios included a case with a sand: clay ratio of 9:1, a case of gravelly sand ground and a case of sandy gravel ground. In the case with gravelly sand ground, ground subsidence could be observed.

Evaluated the behavior of ground subsidence by discharging water and sand through a hole at the center of the bottom of a small soil box with a length of 400 mm, a width of 140 mm and a height of 300 mm. In the above experiment, the results of a centrifugal model experiment and a scale model experiment were compared based on sand ground. In the centrifugal model experiment, a centrifugal acceleration that is 25 times the Earth's gravitational force was applied to the model ground. For the sand ground, a wedge-shaped overall failure behavior was observed in the scale model experiment. In the centrifugal model experiment, a wedge-shaped failure was observed at the upper part of the ground and a narrow box-shaped failure behavior was observed at the lower part of the ground, as shown in Fig. 1.

Sato and Kuwano (2015) observed the ground subsidence mechanism by discharging water and earth/sand through the bottom hole of a model ground in the presence of an underground structure. In the above experiment, leakage occurred through the bottom hole of the model soil box when there was an underground structure above the bottom hole of the model soil box as shown Fig. 2b and c. The leakage occurred as water infiltrated into the model ground due to the precipitation occurring at the top of the model ground and flowed to the vicinity of the underground structure. In this regard, the ground subsidence mechanism was the loss of Earth and sand caused by the flow of water. In addition, in the case in which there was no underground structure as shown in Fig. 2a, only the soil above the bottom hole of the model soil box was carried away when other earth and sand were carried away by the groundwater flow that occurred due to precipitation.

Analysis of the electrical characteristics of the sand ground for GPR exploration: Many GPR exploration is a representative method for exploring the Earth's subsurface and it examines shallow underground structures using electromagnetic pulses in the frequency band of 10 MHz-1 GHz. In this method, the reflection and diffraction of electromagnetic waves due to the permittivity difference between media are measured and geological structures are identified by interpreting the measurement result. The GPR exploration has a relatively high applicability for the exploration of dry sandstone or conglomerate due to its accessible transmission of

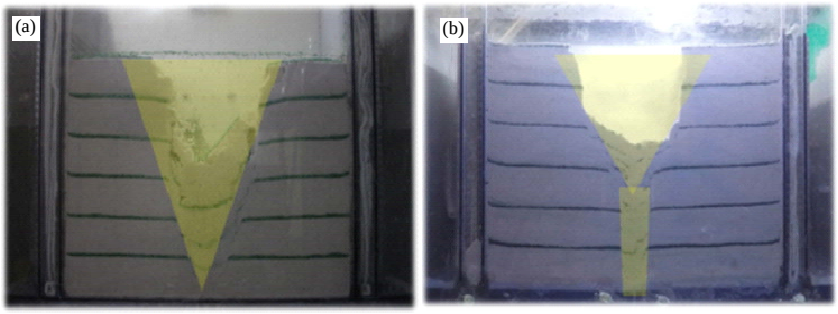

Fig. 1: Behavior difference between the (a) Scale model experiment and (b) Centrifugal model experiment based on sand ground

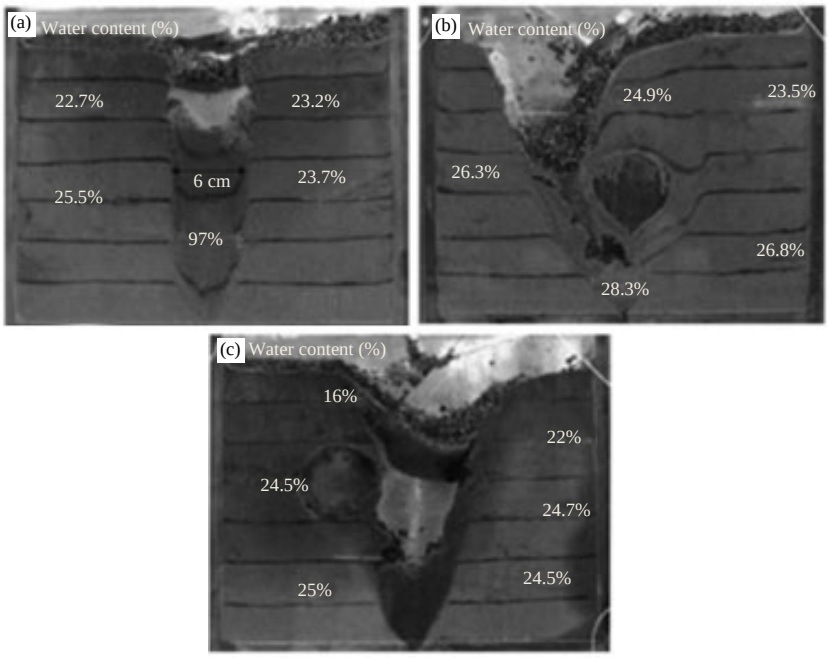

Fig. 2(a-c): Difference in the ground subsidence mechanism depending on the presence of an underground structure within the model ground (Sato and Kuwano, 2015)

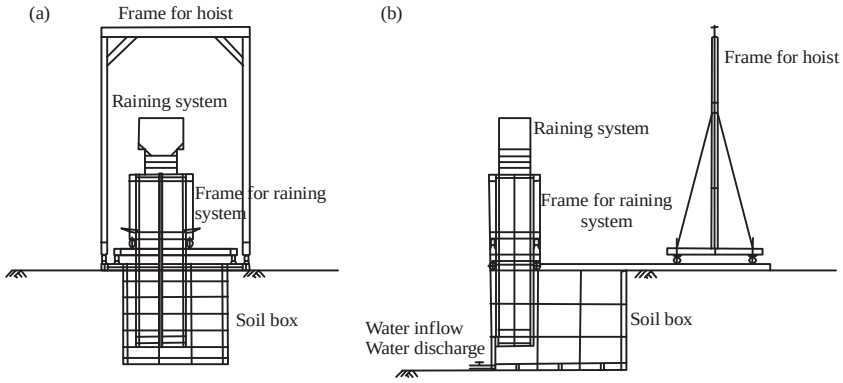

Fig. 3: Conceptual diagram of scale model test (a) Front and (b) Side view

electromagnetic waves. However, it is difficult to apply GPR exploration to a clay layer because the attenuation of electromagnetic waves, depending on the depth can be large due to high electric conductivity. The factors affecting GPR signals include electromagnetic characteristics such as permittivity, electric conductivity and transmittance. To measure the dielectric constant and electric conductivity of sand ground for this study, a model experiment by adjusting the relative density was performed.

A scale model was created as shown in Fig. 3 to examine the various and complex factors of the Earth and to measure the electrical properties of the earth. The scale model was created using acrylic boards to form a chamber measuring a length of 2.1 m, a width of 1.5 m and a height of 1.5 m. To adjust the looseness or denseness of the sand, a mobile frame installed with a sand showering device capable of forward, backward and side-to-side movement was installed on top of the scale model. The height at which sand fell from this contraption was made to be adjustable. In addition, a water inflow and discharge mechanism was installed on the bottom of the scale model to allow groundwater levels of the formed sand grounds to be adjustable (Fig. 3).

The sample compound used during the tests consisted of 96% sand and 4% silt. The uniformity coefficient of the sample was 4.38 and the coefficient of curvature

of the sample was 1.63. According to the unified soil classification system, the sample was classified as SP (Fig. 4).

In the model experiment based on loose sand ground and dense sand ground, sensors for measuring the electrical characteristics and measurement cans for estimating the relative density of sand were arranged as shown in Fig. 5.

To describe the loose sand ground, sand was installed at an interval of 30 cm per layer and the sand ground was formed by allowing sand particles to fall freely through a sieve. A GS3 sensor was used as the TDR sensor for measuring the dielectric constant and electric conductivity of the loose sand ground. The GS3 sensor is manufactured by decagon (USA) and can simultaneously measure dielectric constant and electric conductivity. Three TDR sensors were installed (No. 1: 0.3 m, No. 2: 0.6 m, No. 3: 1.2 m) and dry density measurement cans were installed at the same locations for the estimation of the relative density of the ground.

To simulate sand ground in a dense state, the sand was compacted using a tamping board upon laying each sand layer measuring 30 cm per layer. A plywood board (1.05×0.75 m) that constituted 1/4 of the scale model cross section was assembled and used as the tamping board during this process. The board was used 4 times to compact the sand of each 1/4 area of the scale model. The TDR sensors and dry density measurement cans used to measure the dielectric constant and conductivity of the sand ground were installed under the same conditions and in the same three locations (0.3, 0.6, 1.2 m) as those used to simulate the loose sand ground.

Relative density was calculated using Eq. 1 upon inputting the dry density (γ_d), maximum dry density (γ_{dmax}) and the minimum dry density (γ_{dmin}) which were calculated through indoor tests of the samples collected from the scale model test. The minimum dry density and maximum dry density were determined for this study. First, Earth particles were dropped from a height of 10 mm to find the minimum dry density. Then, the Earth placed in a container and pressure and vibration were applied to find the maximum dry density.

$$D_r = (\gamma_{dmax}/\gamma_d)\times(\gamma_d-\gamma_{dmin})/(\gamma_{dmax}-\gamma_{dmin}) \quad (1)$$

Calculation of the relative density of the concerned layer through the dry density, maximum dry density and the minimum dry density found from the sand in a loose state yielded a result of approximately 40%. Calculation of the relative density of the concerned layer through the dry density, maximum dry density and minimum dry density from the sand in a dense state yielded a result of approximately 60% (Fig. 6).

The results of the measurement showed that the dielectric constants were 3.451 for the loose dry sand and

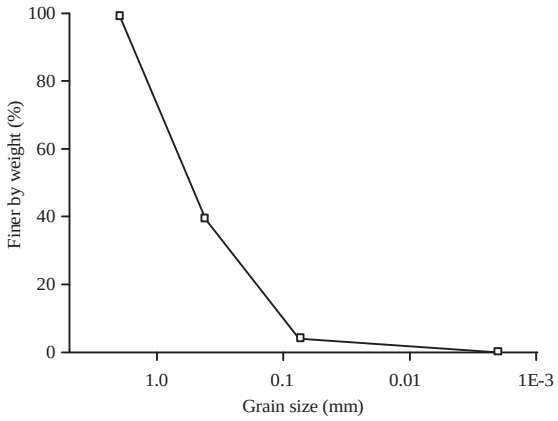

Fig. 4: Grain-size distribution curve

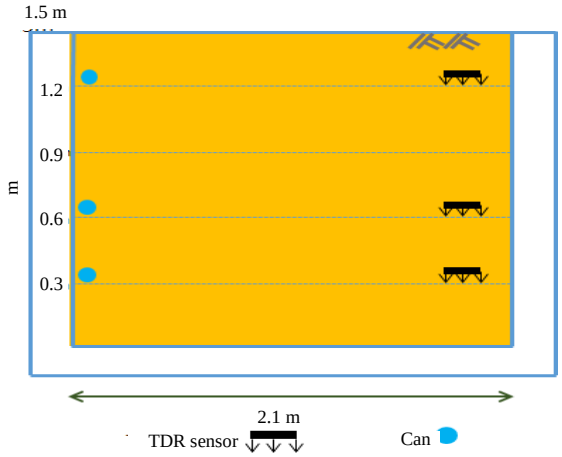

Fig. 5: Section for sensor placement of scale model test

4.245 for the dense dry sand. In the case of the dry sand, the dielectric constant increased as the relative density increased. When the relative density increased, the pores between soil particles became smaller and this decreased the attenuation of the electromagnetic wave energy.

For the saturated sand ground, the measured dielectric constant and electric conductivity were 18.69 and 9.6 mS m^{-1}, respectively (No. 1 in Fig. 7). For the unsaturated sand ground, the values were 7.813 and 4.5 mS m^{-1}, respectively (No. 2 in Fig. 7). The dielectric constant and electric conductivity increased as the moisture content increased with their values converging after 8 days. In this regard, the moisture content converged because the water adsorbed by surface tension continuously ascended up to the capillary rise height. However, it could not fill all the gaps of the soil which was completely saturated up to a certain height above the water level similar to that of the soil below the groundwater level. Thus, the adsorbed water entered an

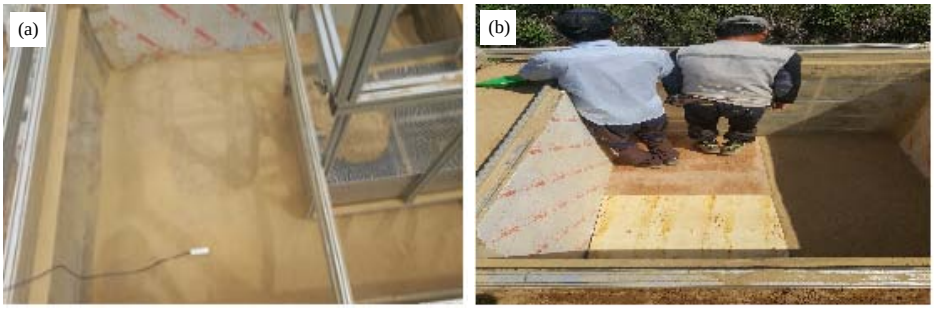

Fig. 6: View for scale model test of sand (a) Loose sand formation and (b) Dense sand formation

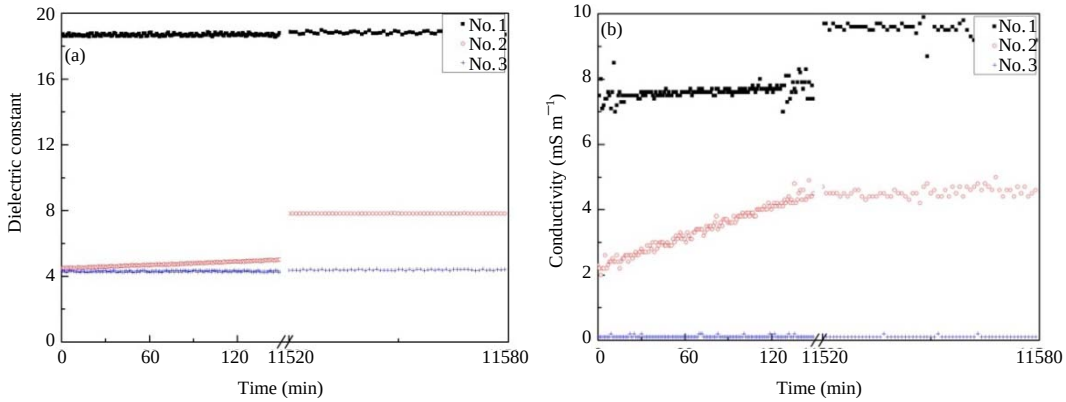

Fig. 7: Electrical characteristics due to capillary rise (a) Dielectric constant and (b) Conductivity

unsaturated condition as the degree of saturation decreased due to the introduction of air above the completely saturated zone.

Water content ratios changed according to the height of capillary rise and such changes were found to largely affect the dielectric constant and conductivity values.

To predict the soil-water characteristic curve of sand that was similar to the sample used in the tests, sand having a coefficient of permeability of 4.3×10^{-6} m sec^{-1} when saturated as indicated by Bruch (1993) was applied to the indoor tests. The acquired data was then applied to Eq. 2 which was proposed by Fredlund and Xing (1994) and was used to present the water characteristic curve. Using this water characteristic curve, the characteristics of the capillary suction forces regarding the saturated and unsaturated sand were analyzed. The volumetric water content calculated during this process was calculated upon applying it to Eq. 3 which regarded the relation between Volumetric Water Content (VWC) and the dielectric constant (ε) as proposed by Decagon Devices, Inc. (2016) through tests:

$$\theta_w = \theta_S/\{In[e+(\psi/a)^n]\}^m \quad (2)$$

Where:

θ_w : The volumetric water content
θ_S : The saturated volumetric water content
e : The natural number 2.71828
Ψ : The negative pore-water pressure
a, n, m : Curve fitting parameters

$$VWC\ (m^3/m^3) = 5.89\times10^{-6}\times\varepsilon^3-7.62\times10^{-4}\times\varepsilon^2+3.67\times10^{-2}\times\varepsilon-7.52\times10^{-2} \quad (3)$$

The volumetric water content of the completely dry sand at a loose state was 4.3% and the volumetric water content of the saturated sand was 38.3%. In addition, the dielectric constant of the unsaturated sand having a capillary rise of 10 cm was 7.813 and the volumetric water content was 16.8%. As indicated in Fig. 8, capillary suction was estimated to be 430 kPa.

Analysis of the limitation of GPR exploration based on simulation: The GPR exploration method can be classified into three types depending on whether the exploration mode used is reflection mode, CMP (Common Midpoint Mode) or transillumination mode. It can also be classified as a single-channel method and a multi-channel method depending on the antenna usage channel. The reflection mode is the most common method

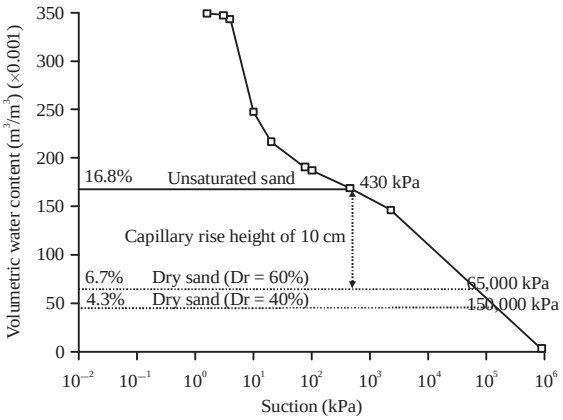

Fig. 8: Soil-Water Characteristic Curve (SWCC)

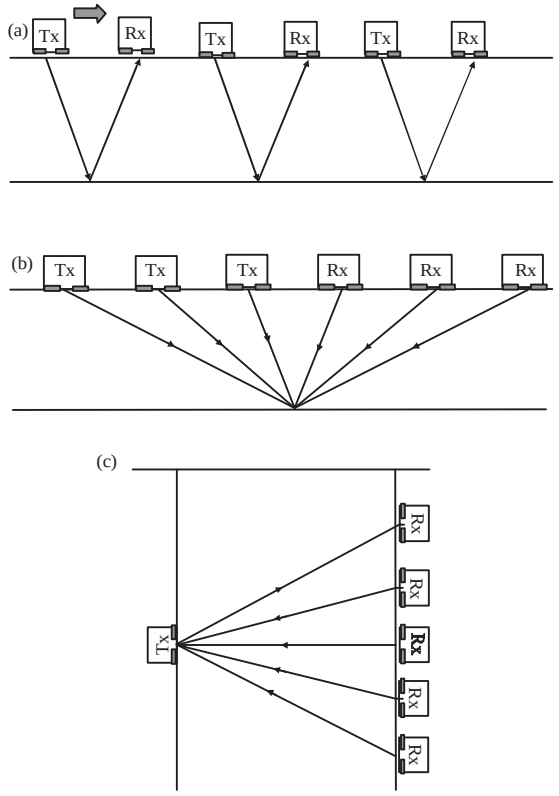

Fig. 9: Exploration mode of GPR (a) Reflection mode (b) CMP (Common Midpoint Mode) and (c) Transillumination mode

for ground survey where a transmitter and a receiver are fixed at a constant interval and the survey is conducted by moving them at regular intervals (X) Fig. 9a. In the CMP mode, the survey is performed by spreading the interval between a transmitter and a receiver at regular intervals. When the CMP mode is used, the propagation speed of electromagnetic waves within ground can be obtained and

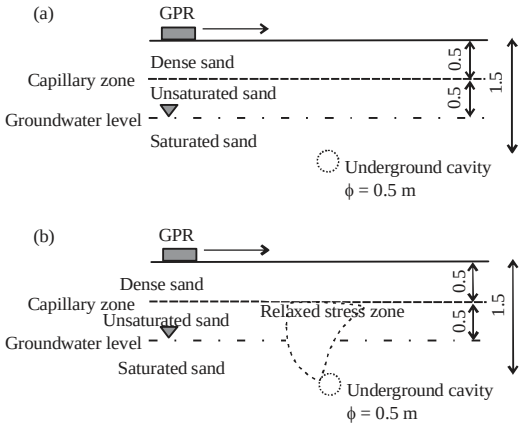

Fig. 10: Modeling for analysis of GPR (a) Case 1 and (b) Case 2

thus, the distance to a target can be accurately analyzed Fig. 9b. The transillumination mode can be used for the surveying of cracks within a pier or the column of a building. This method is different from the reflection mode in that the penetrated waves are received rather than reflected. The principle by which the transillumination mode operates is identical to that of geotomography which performs the imaging of underground sections by making a borehole Fig. 9c.

In the present study, an underground cavity below the ground was described. A simulation was conducted using GPRSIM V3.0 and the reflection mode was used based on the conditions shown in Fig. 9. In Fig. 10a Case 1, an underground cavity below the ground was described for a sand layer and the capillary rise height depending on the groundwater level was considered. In Fig. 10b Case 2, a relaxed ground zone depending on the change in groundwater level was described.

The sequence for the analysis of GPRSIM consisted of model drawing and grid generation, antenna impulse response setting, antenna directionality response setting, wave-type setting of the model, antenna reception and transmission location setting and starting simulation.

The size of the model was 10.0×5.0 m and the number of grids for the finite difference was 200×100. The size of the grid was 5 cm and a constant interval was maintained. Table 1 summarizes the dielectric constant and electric conductivity depending on the ground condition. A direct-reflected wave with a source center frequency of 800 MHz was used.

The results of the GPR exploration simulation (Fig. 11) indicated that the boundary between the unsaturated and saturated grounds of the sand layer showed a difference under high frequency as electromagnetic waves were reflected due to the permittivity difference.

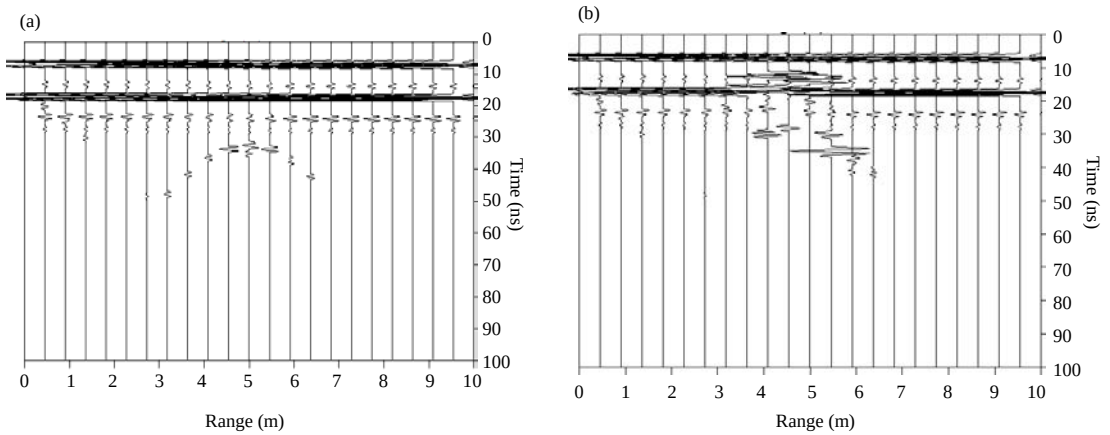

Fig. 11(a-b): Simulation result (a) Case 1 and (b) Case 2

Table 1: Dielectric constant and conductivity of sand

Conditions of sand	Dielectric constant (ε)	Conductivity (mS m^{-1})
Dry		
Loose sand (Dr = 40%)	3.451	0.1
Dense sand (Dr = 60%)	4.245	0.1
Saturated sand	18.690	9.6
Unsaturated sand (Capillary rise height of 10 cm)	7.813	4.5

Below the groundwater level, the attenuation of electromagnetic waves was large due to high electric conductivity. An underground cavity shape with a 0.5 m diameter that is located 1.5 m below the ground showed a parabolic form Fig. 11a. A slight parabolic form was observed due to the overlapping of reflected signals when the vicinity of the underground cavity was relaxed depending on the groundwater level change Fig. 11b.

CONCLUSION

In this study, an underground cavity below the ground was described and a GPR exploration simulation was conducted for the relaxed ground zone depending on the groundwater level change. The following conclusions were obtained. The dielectric constant of the dry sand at a loose state was calculated as 3.451. The dielectric constant of the dry sand at a dense state was calculated as 4.245. In dry sand, the dielectric constant increased as relative density increased, the dielectric constant and conductivity of the saturated sand was 18.69 and 9.6 mS m^{-1}, respectively. The dielectric constant and conductivity of the unsaturated sand having a capillary rise height of 10 cm increased with the passing of time and converged to 7.813 and 4.5 mS m^{-1}, respectively, the volumetric water content of the unsaturated sand having a capillary rise height of 10 cm was 16.8%. Capillary suction at this point was estimated to be 430 kPa, conductivity values reacted sensitively to changes in water content ratios. Greater levels of water content resulted in both greater attenuation of propagated wave energy levels and increased conductivity in the sand layer, the boundary between the unsaturated and saturated grounds could be distinguished due to the permittivity difference, below the groundwater level the attenuation of electromagnetic waves was large due to high electric conductivity, the result of the GPR exploration simulation showed that the underground cavity below the ground had a distinct underground cavity shape and it was difficult to analyze the shape of the underground cavity when the relaxed zone near the underground cavity below the ground became larger depending on the groundwater level change.

ACKNOWLEDGMENT

This study was supported by the Korea Agency for Infrastructure Technology Advancement under the Ministry of Land, Infrastructure and Transport of the Korean Government. (Project Number: 19SCIP-B108153-05).

REFERENCES

Bruch, P.G., 1993. A laboratory study of evaporative fluxes in homogeneous and layered soils. MSc Thesis, Department of Civil Engineering, University of Saskatchewan, Saskatoon, Canada.

Decagon Devices Inc., 2016. GS3 water content, EC and temperature sensors. Decagon Devices Inc., Pullman, Washington, USA. http://library.metergroup.com/Manuals/20429_GS3_Web.pdf

Fredlund, D.G. and A. Xing, 1994. Equations for the Soil-water characteristic curve. Can. Geotech. J., 31: 521-532.

Han, Y. and H.W. Hwang, 2017. Discussion on the sinkhole forming mechanism. Intl. J. Adv. Sci. Eng. Technol., 5: 42-44.

Han, Y., 2018. Proposal of the development direction on the special act on underground safety management for preparation of the proactive underground safety management system. J. Korean Geotech. Soc., 34: 17-27.

Kweon, G., S. Kim and S. Hong, 2016. Basic study on mechanism of cave-in in road through laboratory model tests. Intl. J. Highway Eng., 18: 11-19.

Oh, D.W., H.Y. Ahn and Y.J. Lee, 2016. A study for influence range of ground surface due to sewer fracture in various relative density of sand by laboratory model test. J. Korean Geotech. Soc., 32: 19-30.

Reynolds, J.M., 2011. An Introduction to Applied and Environmental Geophysics. 2nd Edn., Wiley Publishing Company, Hoboken, New Jersey, USA., ISBN:978-0-471-48535-3, Pages: 710.

Sato, M. and R. Kuwano, 2015. Influence of location of subsurface structures on development of underground cavities induced by internal erosion. Soils Foundations, 55: 829-840.